Available online at www.sciencedirect.com

jmr&t Journal of Materials Research and Technology

journal homepage: www.elsevier.com/locate/jmrt

Original Article

Improving the elevated-temperature mechanical properties of AA3004 hot-rolled sheets by microalloying with Mo and optimizing the process route

K. Ma [a,b], E.M. Elgallad [a,*], Z.X. Chen [a], B.L. Xiao [b], X.-Grant Chen [a,**]

[a] Department of Applied Science, University of Québec at Chicoutimi, Saguenay, Québec G7H 2B1, Canada
[b] Shi-changxu Innovation Center for Advanced Materials, Institute of Metal Research, Chinese Academy of Science, 72 Wenhua Road, Shenyang, 110016, China

ARTICLE INFO

Article history:
Received 3 March 2022
Accepted 30 June 2022
Available online 5 July 2022

Keywords:
Al–Mn–Mg 3004 alloy
Microstructure evolution
Elevated-temperature properties
Mo addition
Hot rolling

ABSTRACT

The present work investigated the influence of Mo addition and thermomechanical process routes on microstructural evolution and elevated-temperature mechanical properties of Al–Mn–Mg 3004 alloys. Various combinations of heat treatment and hot rolling were applied to fabricate hot-rolled sheets. The results revealed that microalloying with Mo and two-step heat treatment increased the number density and volume fraction of dispersoids and decreased the volume fractions of dispersoid-free zones. The different processing routes had important impacts on microstructural evolution. The alloys processed with heat treatment followed by hot rolling had finer and better distributions of dispersoids than those subjected to hot rolling prior to heat treatment. The former resulted in higher tensile strengths at room and elevated temperatures. Among all conditions, the Mo-containing alloy subjected to two-step heat treatment followed by hot rolling exhibited the highest elevated-temperature properties and reached a yield strength of 93 MPa at 300 °C. Both the base and Mo-containing alloys subjected to two-step heat treatment followed by hot rolling showed excellent thermal stabilities up to 350 °C and almost no significant change in yield strengths after thermal exposure at 300–350 °C for 100 h.

1. Introduction

With the current development of the automotive and aerospace industries, cost-effective lightweight materials with desired elevated-temperature properties are increasingly in demand [1–4]. Al alloys are excellent candidate materials for lightweight applications, which may involve high-temperature exposure, such as in fire-resistant structures and heat exchangers [5,6]. However, most of the conventional

* Corresponding author.
** Corresponding author.
E-mail addresses: Emad_Elgallad@uqac.ca (E.M. Elgallad), XGrant_Chen@uqac.ca (X.-G. Chen).
https://doi.org/10.1016/j.jmrt.2022.06.171

high strength aluminum alloys, including 2 xxx, 6 xxx and 7 xxx alloys, have low strengths at elevated temperatures due to coarsening of precipitates after thermal exposure [7–9].

Recent studies reported that 3 xxx alloys offered excellent mechanical properties at both room and elevated temperatures due to precipitation of α-Al(MnFe)Si dispersoids [10–13]. The α-Al(MnFe)Si dispersoids were partially coherent with the matrix and had cubic crystal structures [10,14]. Interestingly, the α-Al(MnFe)Si dispersoids proved to be thermally stable at 300 °C, which resulted in enhanced elevated-temperature strength and creep resistance [12,13]. Several attempts were made to optimize the characteristics of α-Al(MnFe)Si dispersoids by addition of alloying elements and/or various heat treatments expected to improve the elevated-temperature mechanical properties of 3xxx alloys [11,13,15–19]. Liu and Chen [12] reported that one-step heat treatment at 375 °C for 48 h promoted precipitation of a large number α-Al(MnFe)Si dispersoids and consequently achieved peak dispersion strengthening of 3004 alloys at 300 °C. Later, a two-step treatment involving heating at 250 °C for 24 h and 375 °C for 48 h was found to significantly improve dispersoid characteristics and both the yield strength and creep resistance at 300 °C compared to the one-step heat treatment at 375 °C for 48 h [17]. Li et al. [13] studied the effects of adding different amounts of Si and Mg on the microstructure and elevated-temperature properties of 3xxx alloys and found that the best elevated-temperature strengthening for α-Al(MnFe)Si dispersoids was attained with 0.25 wt.% Si and 1.0 wt.% Mg. Liu et al. [16] found that an Al–Mn–Mg 3004 alloy with addition of 0.3 wt.% Mo refined the dispersoids and enhanced the thermal stability up to 350 °C.

Dispersoid-free zones (DFZs) always form in interdendrite regions during precipitation heat treatment due to segregation of alloying elements, such as Fe, Si and Mn, during solidification, which decreases the volume fraction of dispersoids and degrades the elevated-temperature properties [11–13]. It is therefore necessary to minimize DFZs when adopting dispersion strengthening. The addition of elements that have a negative segregation ($k_o > 1$) is an effective way to decrease the number of DFZs. Mo was reported to minimize the formation of DFZs in different Al alloys [16,20,21], which resulted in large volume fractions and uniform distributions of dispersoids and ultimately better elevated-temperature properties.

Although previous studies reported promising improvements in the elevated-temperature properties of Al–Mn–Mg 3 xxx alloys as a result of dispersoid strengthening, most investigations were limited on cast ingots. In fact, industrial engineering parts often require materials to undergo large plastic deformations to meet special shape and property requirements. In addition, hot rolling or extrusion can also eliminate casting defects such as slag inclusion and porosity to further improve material properties [22–25]. Zhang et al. [26] found that prerolling at room temperature significantly promoted nucleation of nanosized dispersoids and increased the number density of dispersoids in Al–Mn–Si alloys. However, deformation at room temperature increased the risk of cracking, which increases the difficulty of manufacturing [27]. Therefore, it is necessary to investigate the influence of the hot deformation process on dispersoid microstructures and their related mechanical properties.

The present work was undertaken to investigate the effects of Mo microalloying in combination with a series of process routes, including manipulated heat treatments and hot rolling processes, on the microstructural evolution and mechanical properties of AA3004 rolled sheets. The dispersoid microstructure was characterized under various conditions with optical microscopy (OM) as well as scanning electron microscopy (SEM) and transmission electron microscopy (TEM). Mechanical properties, including microhardness and tensile properties, were evaluated at room temperature and 300 °C. In addition, the thermal stabilities of rolled sheets during prolonged thermal exposure to different temperatures were elaborated.

2. Experimental procedure

Two Al–Mn–Mg 3004 alloys were prepared, including the base alloy free of Mo, in which the main alloying elements (Mn, Si and Fe) were optimized for dispersoid precipitation [12,17], and the other contained 0.22 wt.% Mo. The supplier of metallic elements used to prepare the alloys is Milward Alloys Inc. For each alloy, approximately 5 kg of material was melted in a clay-graphite crucible using an electric resistance furnace. The temperature of the melt was maintained at 750 °C for 30 min. The melt was degassed with pure argon for 15 min and then poured into a permanent steel mold preheated at 250 °C. The dimensions of the cast ingots were 30 × 40 × 80 mm. The chemical compositions of the experimental alloys analyzed with optical emission spectrometer are listed in Table 1.

First, some cast ingots were heat-treated with the one- and two-step procedures developed in references [12,17] to examine microstructural evolution and dispersoid precipitation during heat treatment and provide a benchmark for evaluating the process routes to be developed. The one-step treatment was conducted at 375 °C for 48 h, while the two-step treatment was composed of a first step conducted at 250 °C for 24 h and a second step conducted at 375 °C for 48 h (Table 2). To systematically study the effects of the process routes on the microstructures and mechanical properties, different combinations of heat treatments and hot rolling were applied to both alloys, as detailed in Table 2. The heat treatments were conducted in a programmable air circulating electric furnace. Rolling was carried out on a lab-scale rolling mill with multiple passes at a temperature of ~350 °C. The rolling began from the 26.5 mm-thick ingot and ended with 3.5 mm-thick sheets (85% reduction ratio). Before the mechanical tests, all rolled sheets were subjected to an annealing treatment of 350 °C for 5 h to eliminate the residual stress generated during rolling. To investigate the thermal stabilities of rolled sheets at elevated temperatures, samples subjected

Table 1 – Chemical compositions of the experimental alloys (wt.%).

Alloy	Mn	Mg	Si	Fe	Mo	Al
B	1.55	1.07	0.26	0.28	**0**	Bal.
M	1.54	1.10	0.26	0.29	**0.22**	Bal.

Table 2 – Heat treatments and process routes used with B and M alloys.

Code	Definition
Heat treatments of cast ingots	
B-O	Base alloy; one-step treatment (375 °C/48 h)
B-T	Base alloy; two-step treatment (250 °C/24 h followed by 375 °C/48 h)
M-O	Mo alloy; one-step treatment (375 °C/48 h)
M-T	Mo alloy; two-step treatment (250 °C/24 h followed by 375 °C/48 h)
Process routes with various combinations of heat treatment and rolling	
B-RT	Base alloy; rolling; two-step treatment
M-RT	Mo alloy; rolling; two-step treatment
B-1R2	Base alloy; 1st step treatment (250 °C/24 h); rolling; 2nd step treatment (375 °C/48 h)
M-1R2	Mo alloy; 1st step treatment (250 °C/24 h); rolling; 2nd step treatment (375 °C/48 h)
B-OR	Base alloy; one-step treatment; rolling
B-TR	Base alloy; two-step treatment; rolling
M-OR	Mo alloy; one-step treatment; rolling
M-TR	Mo alloy; two-step treatment; rolling

to selected process conditions were exposed to temperatures of 300, 350 and 400 °C for 100 h before mechanical testing.

After heat treatment or rolling, the samples were polished for metallographic observations using OM and SEM (Jeol, JSM-6480LV). To reveal the general distribution of dispersoids with OM and SEM, the polished samples were etched with 0.5% HF for 30 s. A transmission electron microscope (TEM, Jeol JEM-2100) was used to observe the dispersoids in detail. The thickness of the TEM sample was measured with electron energy loss spectroscopy. The sizes and number densities of the dispersoids were measured using Clemex PE 4.0 image analysis software with TEM images. The volume fractions of dispersoids in the ingots subjected to only heat treatments were calculated according to the following equation [14]:

$$V_{V-H} = A_d \frac{\overline{KD}}{\overline{KD} + t}(1 - A_{DFZ}) \quad (1)$$

where A_d is the area fraction of dispersoids obtained by TEM image analysis; $\overline{D}$ is the average equivalent diameter of dispersoids; t is the TEM foil thickness; A_{DFZ} is the area percentage of dispersoid free zones (DFZs) obtained by OM image analysis; and $\overline{K}$ is the average shape factor of dispersoids, which was taken as 0.42 [14].

During rolling, dispersoids can precipitate in previous DFZs, in which the number densities of dispersoids are generally less than those in dispersoid-rich zones (DRZs); hence, they are redefined as dispersoid-poor zones (DPZs). To calculate the volume fractions of dispersoids in rolled sheets, it is therefore necessary to consider the dispersoids in both DRZs and DPZs using the following modified equation:

$$V_{V-ROLL} = A_{d-DRZ} \frac{\overline{KD_{DRZ}}}{\overline{KD_{DRZ}} + t}(1 - A_{DPZ}) + A_{d-DPZ} \frac{\overline{KD_{DPZ}}}{\overline{KD_{DPZ}} + t} \quad (2)$$

where A_{d-DRZ} is the area fraction of dispersoids in the DRZs; A_{d-DPZ} is the area fraction of dispersoids in the DPZs; $\overline{D}_{DRZ}$ is the average equivalent diameter of dispersoids in the DRZs; $\overline{D}_{DPZ}$ is the average equivalent diameter of dispersoids in the DPZs; and A_{DPZ} is the area percentage of the DPZs. The number density of dispersoids, N_V, which is defined as the number of dispersoids per unit volume, was calculated according to the following equation [15]:

$$N_v = \frac{N}{A(\overline{D} + t)} \quad (3)$$

where N is the number of dispersoids in the TEM image and A is the area of the image; the other parameters, $\overline{D}$ and t, are as defined previously for Eq. (1).

Vickers microhardness measurements were performed on polished samples at room temperature using an NG-1000 CCD microhardness tester with a load of 25 g and a dwell time of 30 s. The tensile properties of rolled sheets were measured at room temperature using an Instron 8801 servo-hydraulic unit at a strain rate of 0.5 mm/min. Tensile properties were measured at 300 °C using a Gleeble 3800 thermomechanical simulator with a strain rate of 10^{-3} s^{-1}, in which the samples were preheated to 300 °C at a heating rate of 2 °C/s and held for 3 min prior to tensile loading. The tensile samples were machined from rolled sheets in the rolling direction with thicknesses of 3 mm, widths of 6 mm and lengths of 25 mm in the gauge area, according to ASTM standard E8/E8 M-13a.

3. Results

3.1. As-cast and as-heat-treated microstructures of cast ingots

Fig. 1 shows the as-cast microstructures of the experimental alloys. The microstructures were generally composed of Al cells as the matrix with dominant Al_6(MnFe) and minor Mg_2Si intermetallic phases distributed in the interdendrite regions. The microstructure of the M alloy was similar to that of the base B alloy [16]. No Mo was detected in the Al_6(MnFe) intermetallics, and no primary Al–Mo intermetallic compound was found in the M alloy (Fig. 1b), which indicated that all of the added Mo was dissolved in the Al matrix.

The microstructures after heat treatments are shown in Fig. 2. In both alloys, large numbers of dispersoids were formed in the interiors of the Al grains/cells, and dispersoid-rich zones (DRZs) were built, as shown by the gray regions in the OM images. The dispersoid-free zones (DFZs), which appeared as bright regions outside the DRZs, were generally located in interdendrite regions surrounding the Al_6(MnFe) intermetallic particles. The higher magnification SEM image

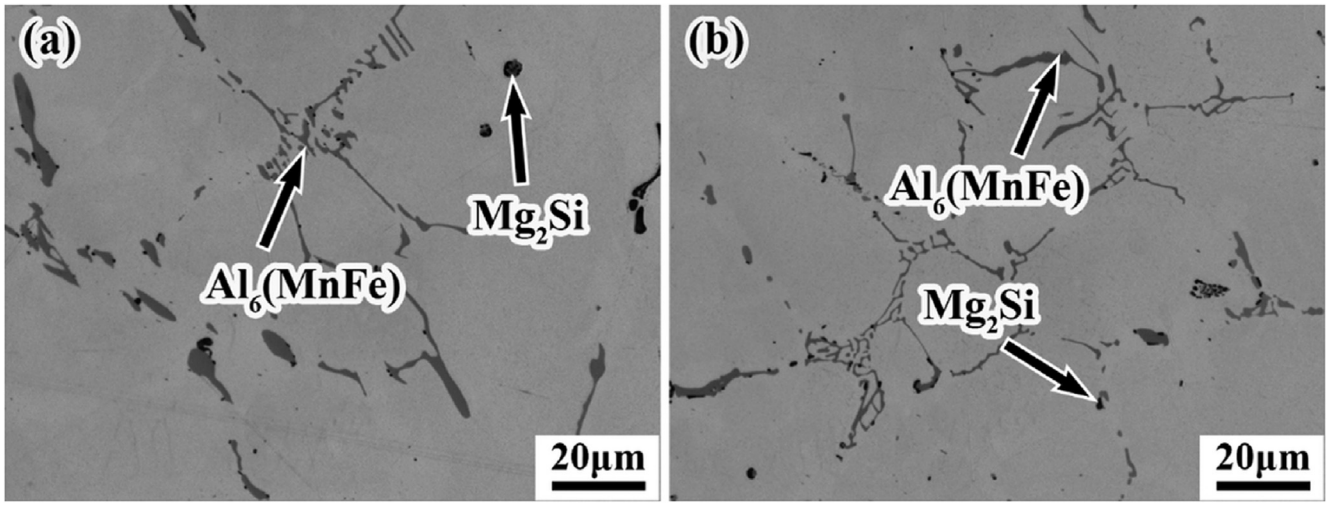

Fig. 1 – As-cast microstructures of (a) B alloy and (b) M alloy.

in Fig. 2e clearly shows the coexistence of the DRZ and DFZ near a primary Al_6(MnFe) particle. The area fractions of DFZs for both alloys subjected to the two heat treatment conditions were quantified based on OM images, as listed in Table 3. This shows proportions of 24.71 vol.% in B–O, 17.28 vol.% in B-T, 14.96 vol.% in M–O and 14.23 vol.% in M-T, respectively. It is apparent that applying a two-step heat treatment and adding Mo decreased the area fraction of DFZs, which agrees well with the findings of Liu et al. [16,17].

The characteristics of dispersoids in the DRZs of B and M alloys after heat treatment were investigated by TEM, and the results are shown in Fig. 3. Dense dispersoids were distributed in the Al matrices in both alloys. The chemical compositions of dispersoids were analyzed using energy dispersive X-ray spectroscopy (EDS)-TEM. The composition of dispersoids in the B alloy (Fig. 3e) matched well with the chemical composition reported for α-Al(MnFe)Si dispersoids [12,14,17]. For the M alloy, the dispersoids were converted from α-Al(MnFe)Si to α-Al(MnFeMo)Si due to the presence of Mo in this alloy (Fig. 3f) [16]. The dispersoids showed similar morphologies in both alloys, which were mainly plate-like and cubic-like, consistent with the morphologies reported for α-Al(MnFe)Si and α-Al(MnFeMo)Si dispersoids [12,13,16]. The insets of Fig. 3a and c shows corresponding selected area electron diffraction patterns (SAEDPs) which are also enlarged in Fig. S1 (see Supplementary Material) revealing faint spots from the dispersoids at $\{110\}_{Al}$ positions [12,14,21]. The sizes, number densities and volume fractions of dispersoids were also quantified, as listed in Table 3. The sizes of dispersoids (equivalent diameters) were nearly the same under all conditions and were approximately 70 nm. The number densities and volume fractions of dispersoids formed in the two-step heat treatment were considerably higher than those of the one-step heat treatment. Moreover, the M alloy had a higher number density and volume fraction of dispersoids than the B alloy under the same heat treatment conditions.

3.2. *Microstructure evolution during various process routes*

Fig. 4 shows typical microstructures for rolled sheets in the B-TR and M-TR conditions as examples of the combinations made. The OM images (Fig. 4a and b) show that all rolled sheets contained gray bands and bright bands associated with intermetallic particles, which were oriented along the rolling direction. The bright bands were the initial interdendrite regions of the cast ingots and were also the DFZs after heat treatment. During rolling, the dispersoids precipitated in these regions to a certain extent. To distinguish the DRZs in the interiors of grains (gray bands), the bright bands are designated dispersoid-poor zones (DPZs), as indicated in the SEM images in Fig. 4c and d. The formation of dispersoids in the bright bands could be attributed to dislocations induced by the large plastic deformations occurring during hot rolling, which promoted dispersoid precipitation [25,28].

The process routes used in this study can be categorized under two main practices, A and B, where the precipitation behaviors of the dispersoids were found to be quite different. In practice A, hot rolling was conducted prior to heat treatment or in between the two steps of the two-step heat treatment, while in practice B, the process routes started with heat treatment followed by hot rolling. The distribution of dispersoids resulting from practice A is shown in Fig. 5. In general, the dispersoid sizes in the DRZs were quite small and averaged approximately 40 nm. In contrast, the dispersoids in the DPZs were significantly larger than those in the DRZs, and their sizes often exceeded 300 nm.

TEM observation was used to determine the sizes, number densities and volume fractions of dispersoids, and these data are listed in Table 4 for all process routes. For the same process route, the M alloy had a higher number density and volume fraction of dispersoids than the B alloy. Furthermore, the number density and volume fraction of dispersoids in the B/M-1R2 conditions were moderately higher than those for the

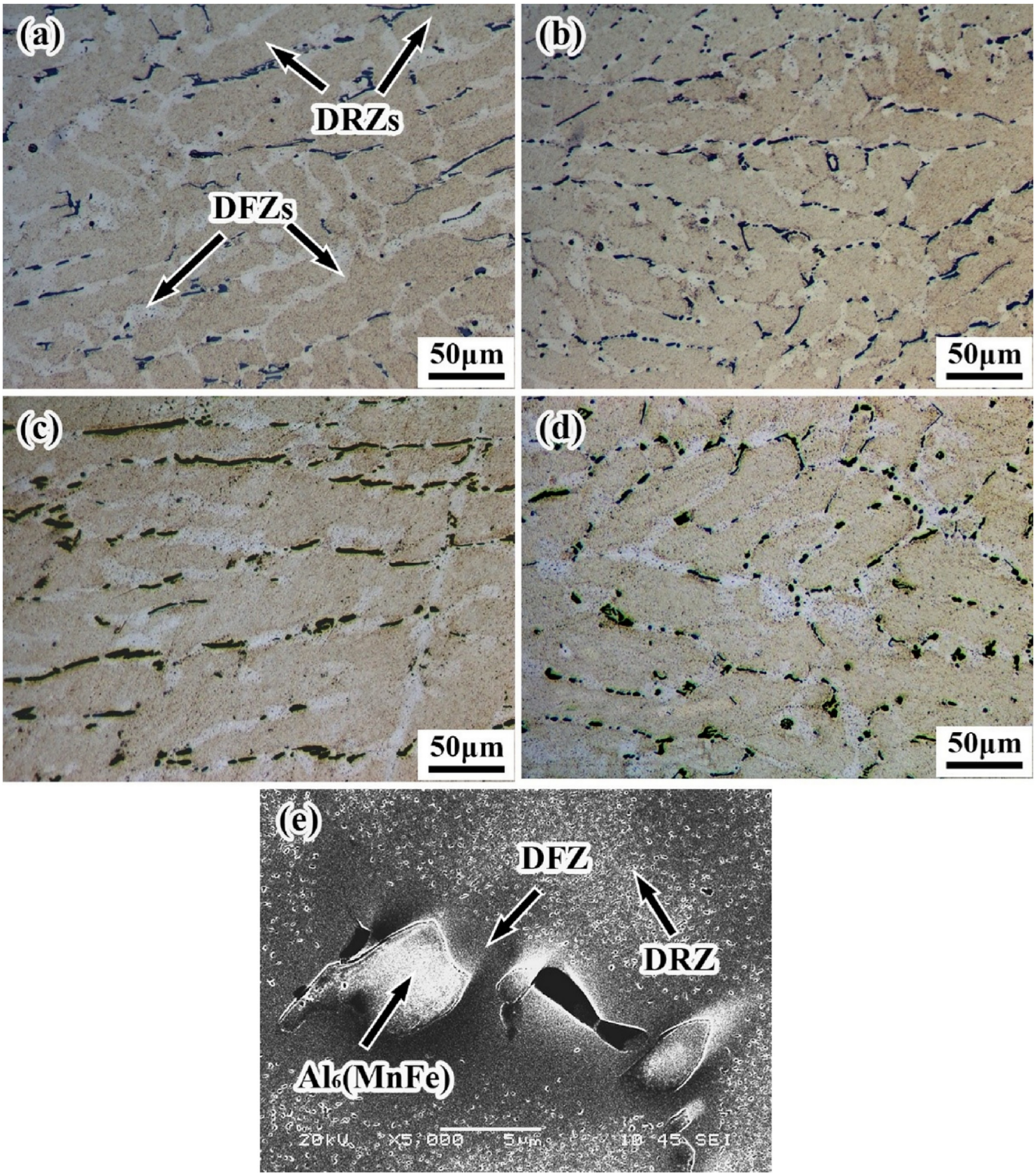

Fig. 2 – Etched microstructures of B and M alloys after heat treatments: (a) to (d) OM images of B–O, B-T, M–O and M-T samples, respectively, and (e) SEM image of a B-T sample.

B/M-RT conditions. This indicated that the first step of the two-step heat treatment in the B/M-1R2 conditions promoted dispersoid nucleation during hot rolling, as β′-Mg_2Si precipitates formed in the first step treatment (250 °C/24 h) could act as potential nucleation sites for dispersoids [17,29]. Under the B/M-RT conditions (first rolling followed by a two-step heat treatment), the rolling temperature was 350 °C, which was much higher than the formation temperature of β′-Mg_2Si

Table 3 – Characteristics of dispersoids formed in B and M alloys with two heat treatments.

Dispersoid characteristics	B-O	B-T	M-O	M-T
Equivalent diameter, nm	66.51	72.07	69.98	67.87
Number density, $\times 10^{19}$ m^{-3}	13.09	16.73	17.61	18.50
Volume fraction, %	2.06	3.28	3.16	3.32
Area fraction of DFZ, %	24.71	17.28	14.96	14.23

precipitates. Instead, α-Al(MnFe)Si dispersoids would be formed during hot rolling, making the subsequent two-step heat treatment less efficient in promoting dispersoid nucleation.

The distribution of dispersoids resulting after conducting practice B is shown in Fig. 6. It is interesting to note that (i) the dispersoid sizes in the DRZs in the B/M-OR and B/M-TR conditions were remarkably smaller than those resulting from heat treatment alone without hot rolling (Fig. 3); and (ii) the dispersoid sizes in the DPZs were much smaller than those from practice A (Fig. 5). The dispersoid characteristics in the case of practice B are also quantified in Table 4. Due to precipitation of small dispersoids in DPZs, the distribution of dispersoids in the Al matrix was more uniform, and the average size of dispersoids was much smaller than those for practice A (B/M-RT and B/M-1R2). Although the volume fractions of the dispersoids in practice B were lower than those in practice A, the number densities of the dispersoids exhibited the opposite tendency. For the same process route, the number densities and volume fractions of dispersoids in the M alloys were higher than those in the B alloys.

3.3. *Mechanical properties of rolled sheets*

3.3.1. *Microhardness*

Fig. 7a shows the microhardness values of the B and M alloys with different heat treatments. The microhardness of either alloy was significantly improved after one-step or two-step heat treatments, which can be attributed to precipitation of large numbers of dispersoids during heat treatments (Fig. 3). Furthermore, the microhardness was higher with the two-step heat treatment than with the one-step heat treatment, and the M alloy had a higher microhardness than the base alloy B under the same heat treatment conditions, which coincides with the corresponding dispersoid characteristics revealed by TEM (Fig. 3 and Table 3).

Fig. 7b shows the microhardness values of the B and M alloys with different process routes. The microhardness values of the B and M alloys processed with practice B (B/M-OR and B/M-TR) were generally higher compared to those processed with practice A (B/M-RT and B/M-1R2), which is consistent with the TEM observation and dispersoid quantification in terms of the size and number density (Table 4). For the same group of process routes, the hardness differences were small; for instance, the hardness values for the B/M-TR conditions were slightly higher than those for the B/M-OR conditions. Under the same process conditions, the hardness of the M alloy was higher than that of the B alloy due to the higher number densities and volume fractions of dispersoids in the M alloys (Table 4).

3.3.2. *Room- and elevated-temperature tensile properties*

Fig. 8 shows the room- and elevated-temperature yield strengths (YSs) of the B and M alloys with different process routes. The strength evolutions at both room temperature and 300 °C with different process routes showed a trend similar to that of the microhardness results (Fig. 7b). The alloys processed with practice B (B/M-OR and B/M-TR) exhibited higher YSs than those processed with practice A (B/M-RT and B/M-1R2), with an average increase of 31% at room temperature and 17% at 300 °C. Among various process routes, the process route starting with the two-step heat treatment followed by rolling (B/M-TR) led to the best mechanical performance. For a given process route, the YSs of the M alloys were always higher than those of the B alloys. Among all conditions, the M-TR process gave the highest YSs, with a value of 214.7 MPa at room temperature and a value of 92.7 MPa at 300 °C.

The tensile properties (UTS, YS and El) of the B and M alloys at both room temperature and 300 °C with different process routes are listed in Table S1with some typical stress–strain curves shown in Figs. S2 and S3 (see Supplementary Material). As engineering materials applicable under different conditions, both B-TR and M-TR alloys with the two-step heat treatment followed by rolling exhibited excellent combinations of room- and elevated-temperature properties. For instance, the B-TR alloy produced a YS of 183.5 MPa and UTS of 254.4 MPa at room temperature, and a YS of 86.9 MPa and UTS of 97.3 MPa at 300 °C. Comparatively, the M-TR alloy was even better and presented a YS of 214.7 MPa and UTS of 268.1 MPa at room temperature, and a YS of 92.7 MPa and UTS of 101.3 MPa at 300 °C. It is also interesting to mention that in the same process group, the B-OR and M-OR alloys with one-step heat treatment followed by rolling showed slightly lower tensile properties relative to the B-TR and M-TR alloys and still exhibited good combinations of room- and elevated-temperature properties.

3.3.3. *Elevated-temperature tensile properties after different thermal exposures*

To study further the mechanical properties and thermal stabilities of the materials at elevated temperatures, all rolled sheets were exposed to a temperature of 300 °C for 100 h. In addition, selected samples of B-TR and M-TR alloys were also exposed to temperatures of 350 and 400 °C for 100 h. Following thermal exposure, the tensile properties were measured at 300 °C. The YSs after thermal exposure for the B and M alloys treated with different process routes are shown in Fig. 9. After thermal exposure at 300 °C for 100 h (Fig. 9a), almost no change was found in YSs for all alloys and process conditions, and the decreases in YSs were limited to 1–2.7% compared to the initial YSs before thermal exposure (Fig. 8b). With increases in the exposure temperature to 350 and 400 °C, the YSs were moderately decreased for the B-TR and M-TR conditions (Fig. 9b). When compared with the initial YSs before thermal exposure (Fig. 8b), the declines in YSs for the exposure temperatures of 350 and 400 °C were ~7.2 and ~16%, respectively. The tensile properties at 300 °C (UTS, YS and El) after thermal exposures at three different temperatures are listed in Tables S2 and S3 (see Supplementary Material). At 300 °C, the ductility of the material is generally not of primary concern,

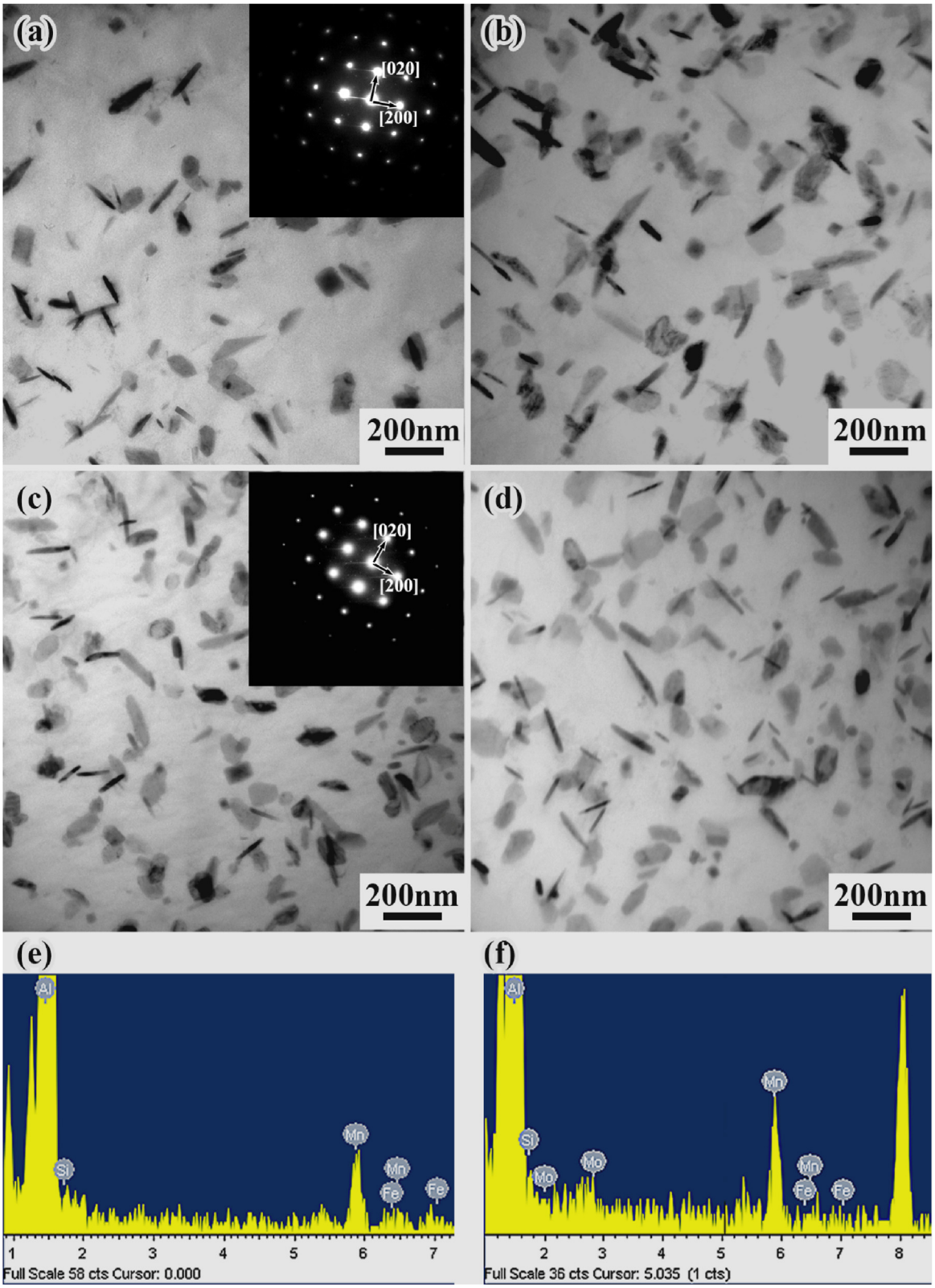

Fig. 3 – Bright-field TEM images for the dispersoids formed in B and M alloys after heat treatments, (a) B–O, (b) B-T, (c) M–O and (d) M-T, and TEM-EDS spectra (e and f) from dispersoids in the B–O and M–O conditions, respectively. The insets of (a) and (c) show corresponding SAEDPs (see also Fig. S1 in Supplementary Material).

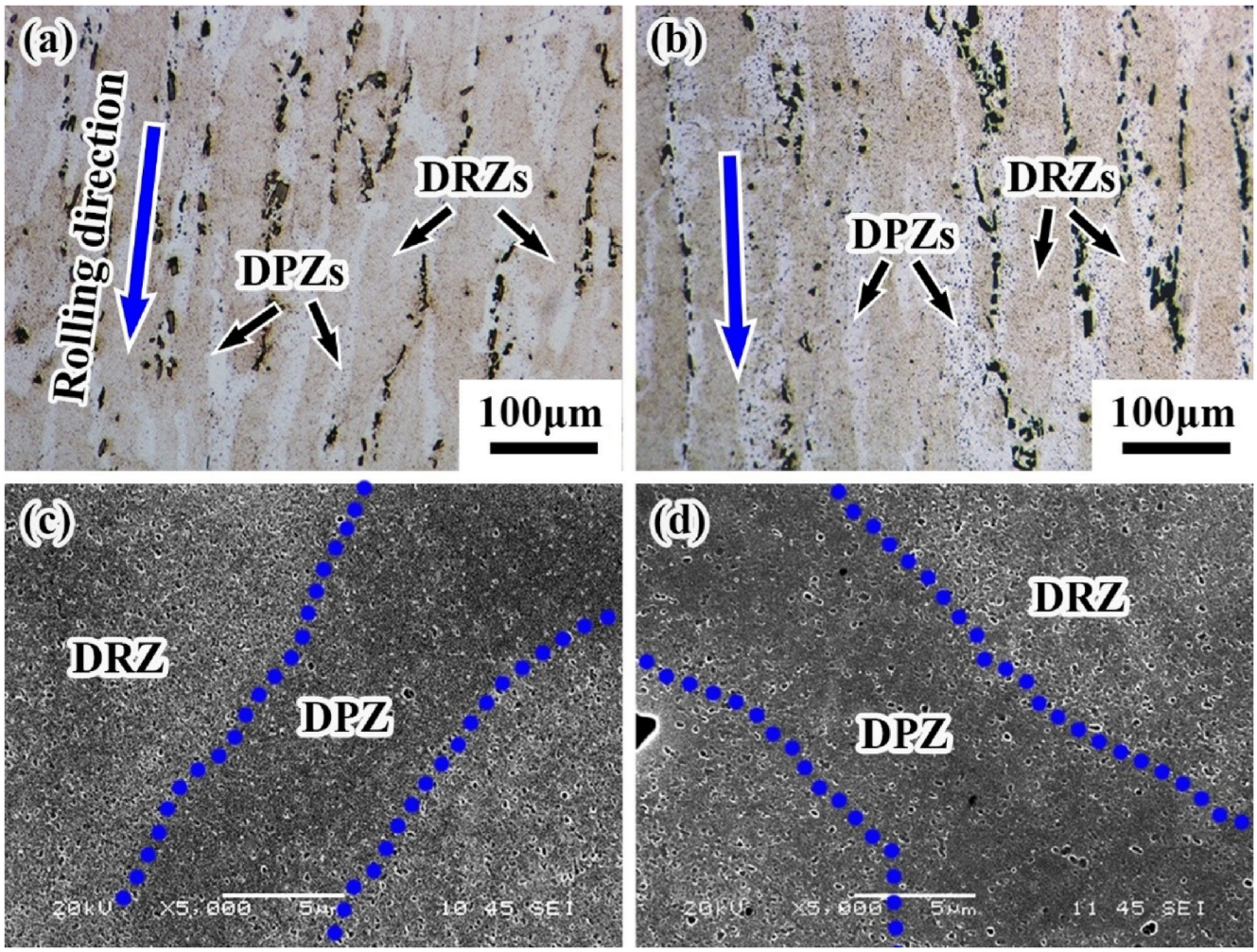

Fig. 4 – Microstructures of rolled sheets: (a) and (c) B-TR; (b) and (d) M-TR.

where the elongation can easily reach 45–55%. The changes in the UTS after thermal exposure exhibited the same trend as the YS. Generally, the data indicated that the hot-rolled materials in the B-TR and M-TR conditions had excellent thermal stabilities up to 350 °C. Even after thermal exposure at 400 °C, the materials still had fair thermal stabilities and exhibited YSs as high as 73–78 MPa at 300 °C, thereby providing reliable safety margins at high service temperatures.

4. Discussion

4.1. *Effect of the process route and Mo microalloying on the microstructure and mechanical properties*

Conventional 3 xxx alloys are non-heat-treatable Al alloys and are strengthened mainly by strain hardening and solid solution hardening. With the optimized chemical composition (Mn, Si, Fe and Mo) used in the present work [12,16,17], the precipitation of a large number of semicoherent α-Al(MnFe)Si dispersoids in the Al matrix was promoted by heat treatment at 375 °C, and thereby dispersoid hardening was the main strengthening mechanism affecting mechanical properties. Because the α-Al(MnFe)Si dispersoids are thermally stable at 300–350 °C [12,16], materials containing such dispersoids would be especially suitable for different applications at elevated temperatures.

The characteristics of dispersoids (size, number density, fraction and distribution) have a great impact on elevated-temperature mechanical properties. It was discovered in the present work that refinement of dispersoids during large plastic deformations (hot rolling) in practice B was particularly promising for improving the distributions of dispersoids and hence enhanced elevated-temperature mechanical properties. Dispersoid refinement was induced by (i) partial dissolution of the existing dispersoids during hot rolling and (ii) dislocation-induced precipitation of new dispersoids in both DRZs and previous DFZs. Dispersoid refinement after severe plastic deformation has been found with other Al alloys [30–34]. Hu et al. [34] investigated precipitate refinement in Al–Cu alloys after severe plastic deformation and found that the mechanism of precipitate refinement was related to the mismatch degree between the precipitates and the matrix. If the precipitates were coherent or semicoherent with the matrix, matrix deformation caused the precipitates to deform together, which resulted in an increase in the free energy of

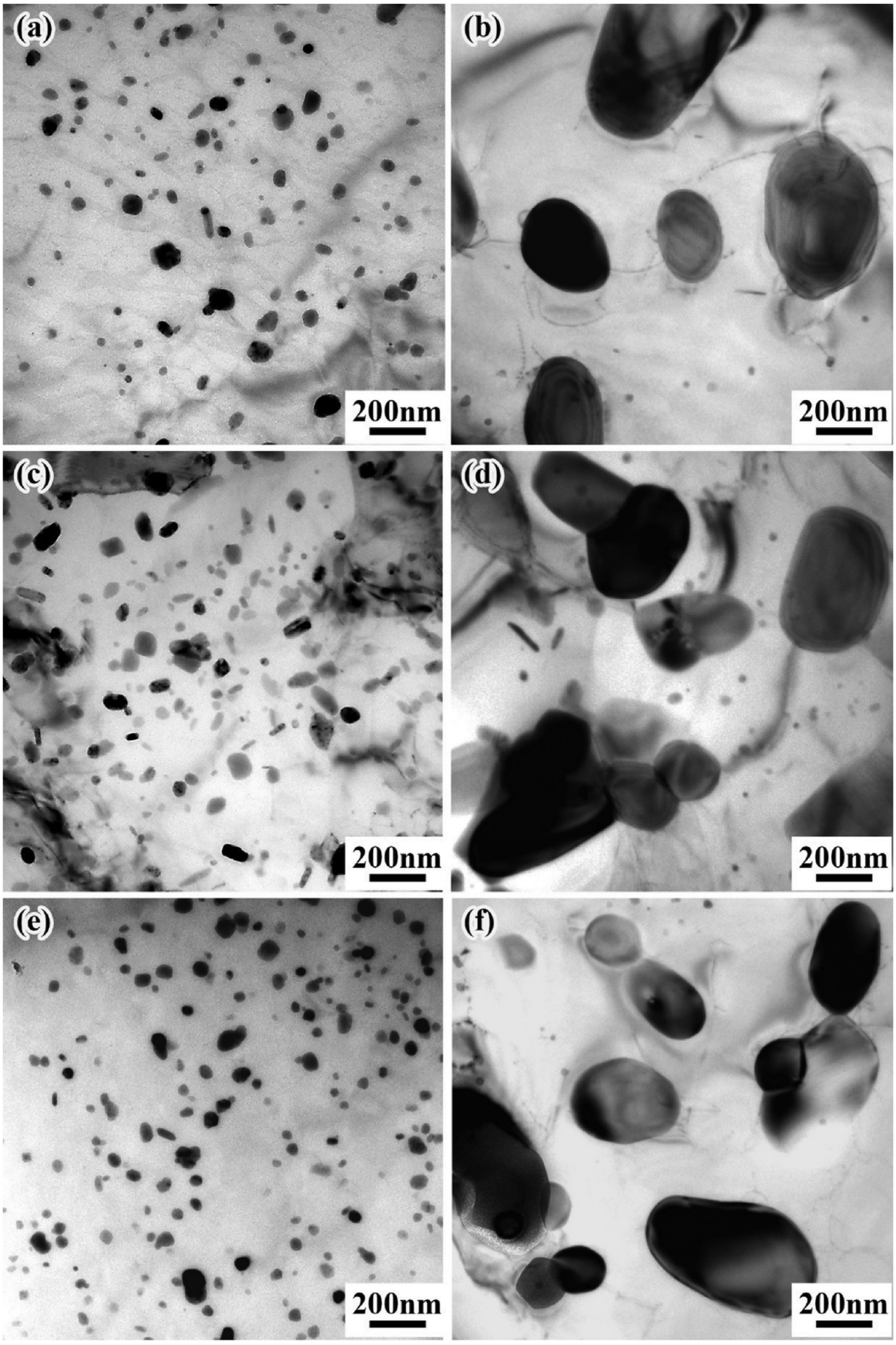

Fig. 5 – TEM images showing the dispersoid distribution after applying practice A: (a) DRZ of B-RT, (b) DPZ of B-RT, (c) DRZ of M-RT, (d) DPZ of M-RT, (e) DRZ of B-1R2, and (f) DPZ of B-1R2.

Table 4 – Characteristics of dispersoids formed in B and M alloys with various process routes.

Dispersoid characteristics	Practice A				Practice B			
	B-RT	M-RT	B-1R2	M-1R2	B-OR	M-OR	B-TR	M-TR
Equivalent diameter in DRZ, nm	40.94	42.82	41.24	42.78	40.84	40.90	41.07	40.10
Equivalent diameter in DPZ, nm	327.93	336.34	326.76	328.27	47.60	48.95	52.27	48.84
Number density, $\times 10^{19}$ m^{-3}	10.51	12.89	12.67	14.98	43.45	48.45	45.06	50.99
Volume fraction, %	4.79	5.07	4.91	5.21	1.76	2.00	1.85	2.12
Area fraction of DPZ, %	37.37	34.38	35.19	32.13	26.12	24.67	24.36	23.15

the system, in which case the precipitates partially dissolved to maintain energetic stability. It was reported that the α-Al(MnFe)Si dispersoids were semicoherent with the matrix [14]. During large plastic deformation (hot rolling), large dispersoids that formed during the preceding heat treatment were partially dissolved. Because the rolling temperature was quite low (350 °C) and there were many dislocations present, new and small dispersoids were formed in both the DRZs and DPZs during hot rolling. Therefore, the dispersoids were smaller, denser and more uniform (Fig. 6a, c and e, Table 4) compared to the dispersoid microstructures generated by heat treatment only (Fig. 3, Table 3).

In contrast, practice A caused precipitation of unusually large dispersoids in DPZs and increases in the fractions of these zones (Fig. 5 and Table 4). During large plastic deformations (hot rolling), heavy stresses were applied on the hard intermetallic particles in the interdendrite boundaries, and a large number of dislocations accumulated in the regions. The abundant dislocations greatly facilitated diffusion of solute elements and consequently promoted precipitation of dispersoids during rolling, and the dispersoids were coarsened during subsequent heat treatment. Therefore, the dispersoids were extremely large in the DPZs, and the fraction of DPZs was enlarged. The dislocations in the grain interiors caused by deformation also promoted dispersoid nucleation. However, dispersoid overgrowth and coarsening in the DPZs consumed large amounts of solute elements. The amount of solute elements in the DRZs in the B/M-RT and B/M-1R2 conditions were therefore less than those in the B/M-OR and B/M-TR conditions, which decreased the driving force for dispersoid precipitation in the DRZs in the case of practice A. Therefore, the strengthening effects of dispersoids at both room and elevated temperatures were much better with practice B than with practice A, as shown in Fig. 8.

Introducing the two-step heat treatment promoted dispersoid precipitation in cast ingots, resulting in a higher number density of dispersoids and a reduction of DFZs compared with the one-step heat treatment (Fig. 3 and Table 3). However, conducting hot rolling between the two steps of heat treatment (B/M-1R2) seemed to provide little advantage (B/M-1R2 *vs.* B/M-RT, Figs. 8 and 9). In addition, refinement effects of the dispersoids in practice B seemed to outweigh the beneficial effects of the two-step heat treatments in the B/M-OR and B/M-TR conditions. Therefore, the strength increments in the B/M-TR samples relative to the B/M-OR conditions were marginal (see Figs. 8 and 9).

After thermomechanical processing, the beneficial effects of Mo microalloying on the dispersoid distribution and mechanical strength were obvious, which is consistent with results of cast ingots in previous works [16,23]. The addition of a small amount of Mo did not change the dispersoid size much but increased the volume fraction of dispersoids and decreased the fraction of DPZs (Table 4). It was confirmed in the present work that, for a given process route, the distributions of dispersoids in M alloys in terms of number density and volume fraction were better than those in B alloys. As a consequence, the elevated-temperature YSs of M alloys were further improved by ~7% relative to those of the B alloys without Mo (Fig. 8b).

4.2. *Thermal stability at elevated temperatures*

As mentioned above, materials containing thermally stable dispersoids can exhibit good elevated-temperature mechanical properties after thermomechanical processing. On the other hand, the thermal stabilities of microstructures and mechanical properties are important for Al alloys used at elevated temperatures. Once a reasonable amount of dispersoids has been formed via different combinations of heat treatment and hot rolling, the rolled sheets are stable and able to operate at temperatures reaching 0.7 T_m (T_m = absolute melting temperature). The results presented in Section 3.3.2. indicated that the mechanical properties resulting after heating at 300 and 350 °C (0.6–0.7 T_m) for 100 h for all process routes were close to the original values seen before thermal exposure (Fig. 9 *vs.* Fig. 8b) due to the thermal stabilities of α-Al(MnFe)Si/α-Al(MnFeMo)Si dispersoids [12,16]. When the exposure temperature reached 400 °C (above 0.7 T_m), the mechanical properties deteriorated slightly due to dispersoid coarsening at such high temperatures. The TEM results shown in Fig. 10 confirmed that the dispersoids formed in the B-TR and M-TR samples after thermal exposure at 400 °C for 100 h were somewhat coarsened. The sizes of the dispersoids increased, and the number densities were reduced to some extent compared with those exhibited before thermal exposure, as shown in Fig. 6c-f. Coarsening of the dispersoids weakened their capacity to hinder dislocation movement, and therefore, the elevated-temperature strengths dropped moderately under these conditions.

It is interesting to note that the dispersoid size in the Mo-containing M-TR sample was still smaller than that in the Mo-free B-TR sample after thermal exposure at 400 °C for 100 h (Fig. 10c and d *vs.* Fig. 10a and b). This result revealed slower coarsening rates of the dispersoids in the Mo-containing M alloy due to the extremely low diffusion rate of Mo present in these dispersoids. Therefore, the Mo-containing M alloys exhibited higher elevated-temperature strengths relative to the base B alloys after thermal exposures between 300 and 400 °C (Fig. 9b).

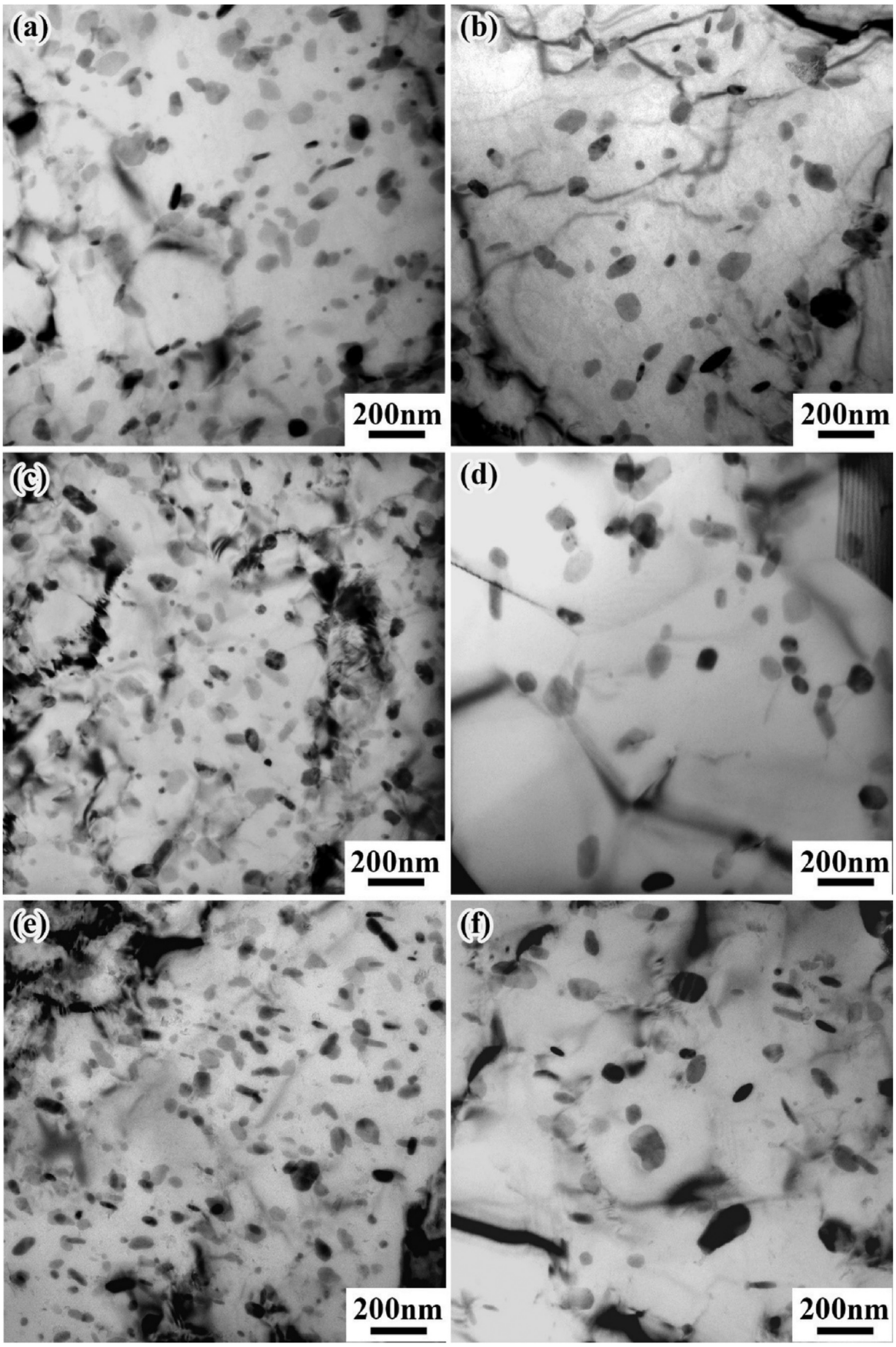

Fig. 6 – TEM images showing the dispersoid distribution after applying practice B: (a) DRZ of B-OR, (b) DPZ of B-OR, (c) DRZ of B-TR, (d) DPZ of B-TR, (e) DRZ of M-TR, and (f) DPZ of M-TR.

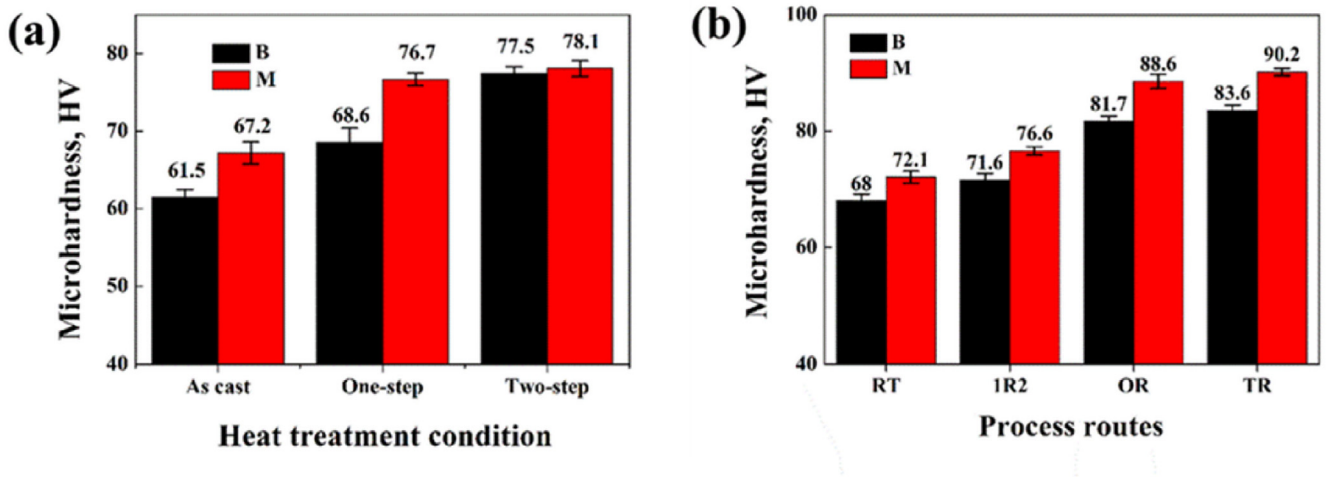

Fig. 7 – Microhardness of B and M alloys with different: (a) heat treatments and (b) process routes.

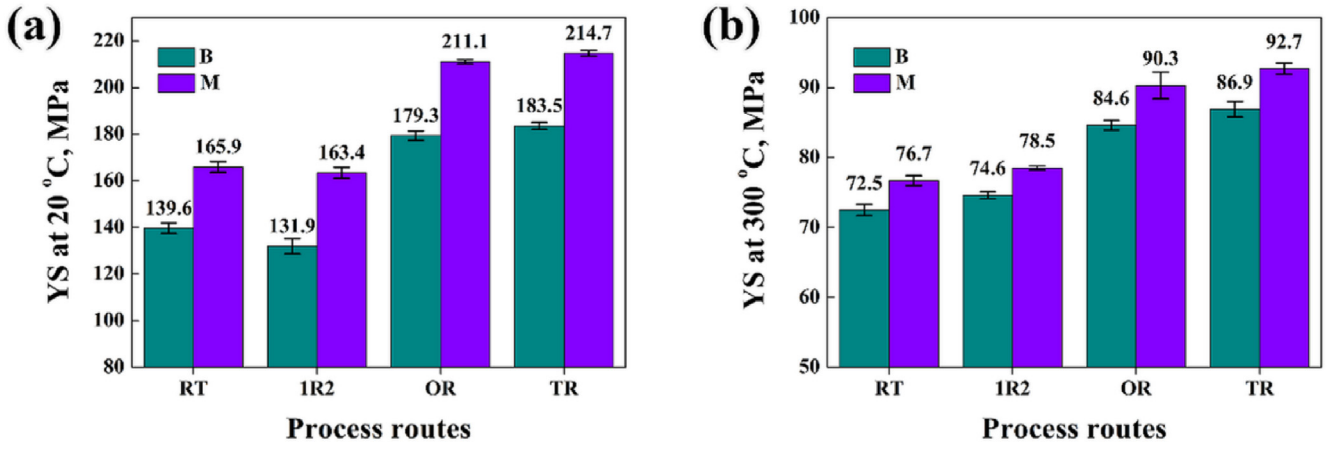

Fig. 8 – Yield strengths (YSs) of B and M alloys with different process routes: (a) at room temperature and (b) at 300 °C.

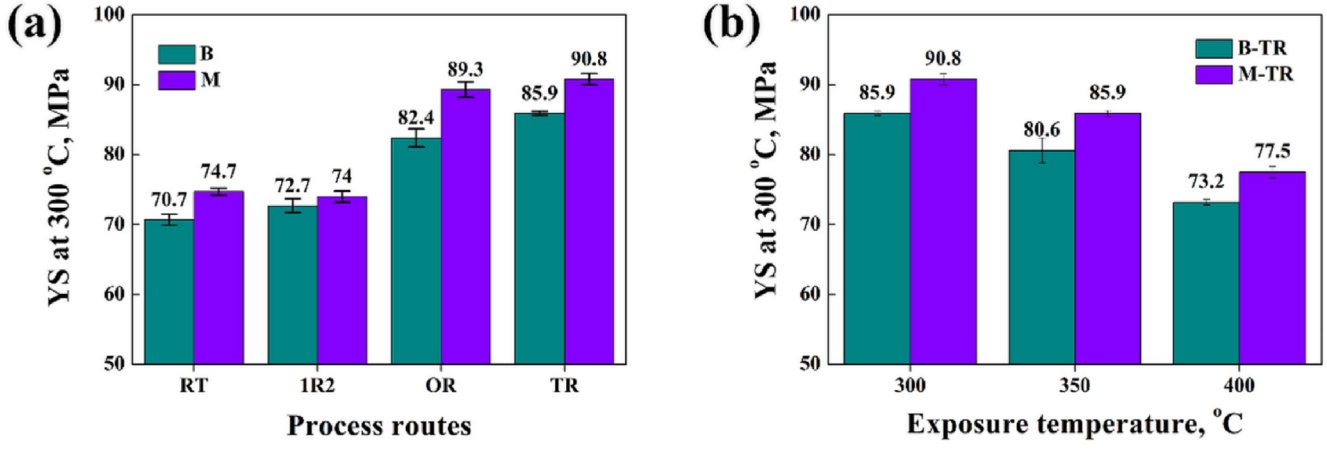

Fig. 9 – Yield strengths (YSs) of B and M alloys at 300 °C: (a) with different process routes after thermal exposure at 300 °C for 100 h, and (b) for B-TR and M-TR conditions after thermal exposures at different temperatures for 100 h.

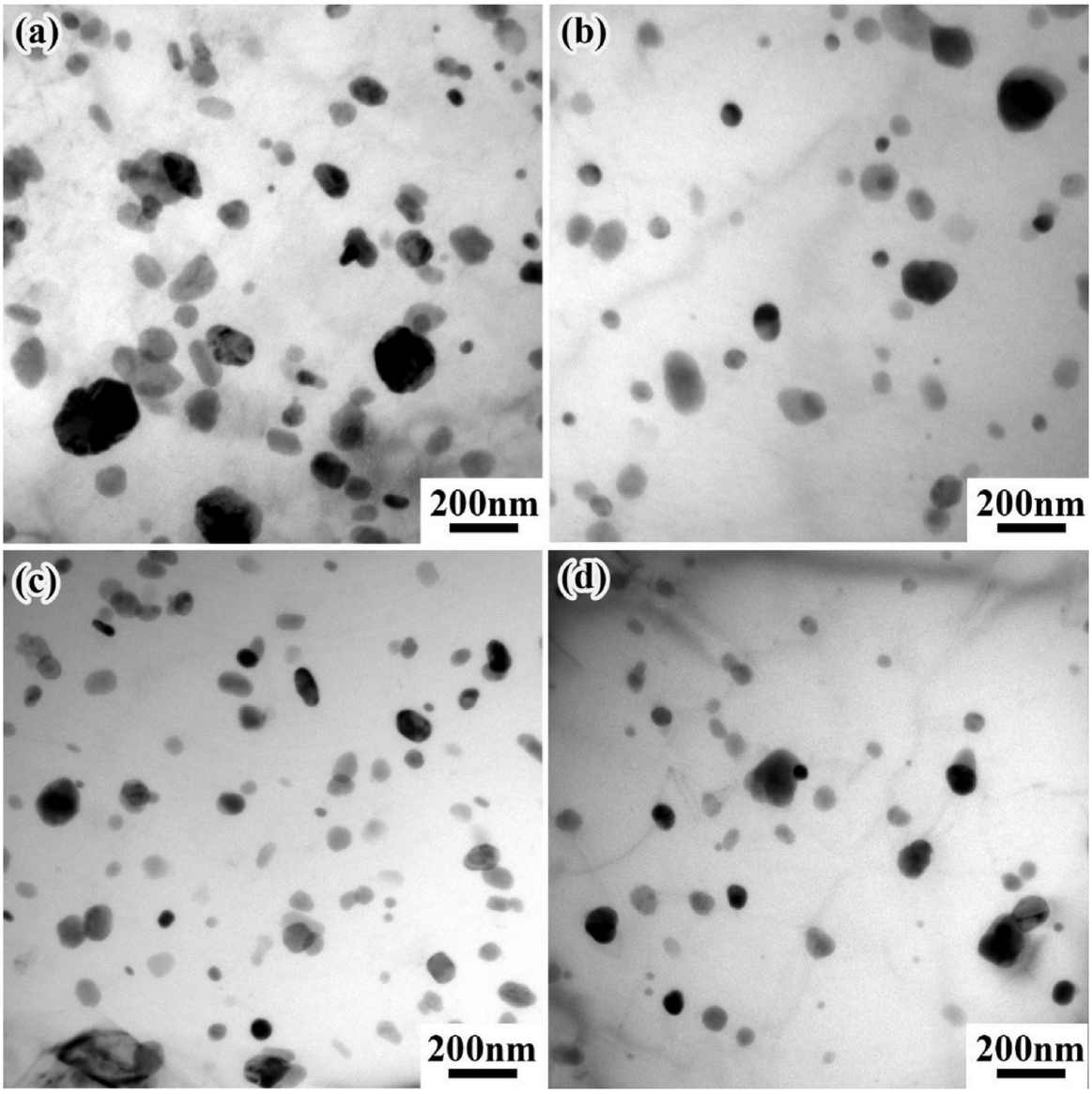

Fig. 10 – Dispersoid distribution after thermal exposure at 400 °C/100 h: (a) DRZ of B-TR, (b) DPZ of B-TR, (c) DRZ of M-TR, and (d) DPZ of M-TR.

In conventional precipitation-hardening Al alloys, such as 2 xxx, 6 xxx and 7 xxx alloys, nanoscale precipitates (Al_2Cu, Mg_2Si and Zn_2Mg types) provide excellent room-temperature mechanical properties. However, once the materials experience high temperatures or use at over-temperatures (>0.5 T_m), the mechanical properties deteriorate dramatically to very low levels due to rapid coarsening of such precipitates. Moreover, this process is irreversible, and the materials can no longer be reused under normal conditions. The results in this study demonstrated that dispersion strengthened materials after optimizing the thermomechanical process and chemistry (M-TR condition) provided high strengths at elevated temperatures (as high as above 90 MPa YS at 300 °C) and excellent thermal stability up to 350 °C. It should also mention that in the conventionally processed AA3004 wrought alloy, the YS at 315 °C after thermal exposure at 315 °C for 100 h was only 41 MPa [35]. The unique engineering advantages of these elevated-temperature sheet products provide a great opportunity to meet the rapidly expanding industrial demand for lightweight Al alloys that are capable of working at either long-term or periodic elevated temperature exposures.

5. Conclusions

In this study, the AA3004 base alloy and its variant micro-alloyed with Mo were cast and processed with various combinations of heat treatments and hot rolling. The microstructures were observed, and mechanical properties were evaluated at room and elevated temperatures. The following conclusions were drawn:

1) Introducing the precipitation heat treatment for non-heat-treatable AA3004 alloys promoted precipitation of

a large number of α-Al(MnFe)Si dispersoids in the interiors of Al grains/cells as a major strengthening phase. Microalloying with Mo and two-step heat treatment increased the number densities and volume fractions of dispersoids and decreased the area fractions of dispersoid-free zones.

2) The processing route significantly affected the characteristics and distributions of dispersoids. For alloys that underwent hot rolling prior to heat treatment (practice A), the dispersoids were substantially coarsened, while for the alloys that underwent heat treatment followed by hot rolling (practice B), the dispersoids were refined, and their distribution in the matrix was more uniform.
3) The alloys processed with practice B exhibited higher tensile strengths at both room and elevated temperatures than those processed with practice A, with average increases in yield strength of 31% at room temperature and 17% at 300 °C. Among all conditions, the Mo-containing alloy subjected to the two-step heat treatment followed by hot rolling exhibited the highest yield strengths of 215 MPa at room temperature and 93 MPa at 300 °C because it showed the best number density, volume fraction and distribution of dispersoids.
4) Both the base and Mo-containing alloys subjected to the two-step heat treatment followed by hot rolling had excellent thermal stabilities up to 350 °C. After thermal exposure to 300–350 °C for 100 h, almost no significant changes were observed in elevated-temperature yield strengths. With an increase in the thermal exposure temperature to 400 °C, the yield strengths deteriorated slightly due to dispersoid coarsening.

Declaration of Competing Interest

The authors declare the following financial interests/personal relationships which may be considered as potential competing interests: X.-Grant Chen reports financial support was provided by Natural Sciences and Engineering Research Council of Canada (NSERC) and Rio Tinto Aluminum, through the NSERC Industry Research Chair in Metallurgy of Aluminum Transformation at the University of Quebec at Chicoutimi.

Acknowledgments

The authors would like to acknowledge the financial support from the Natural Sciences and Engineering Research Council of Canada (NSERC) and Rio Tinto Aluminum under the Grant No. CRDPJ 514651-17 through the Research Chair in Metallurgy of Aluminum Transformation at the University of Quebec at Chicoutimi. K. Ma would like to acknowledge the support from China Scholarship Council.

Appendix A. Supplementary data

Supplementary data to this article can be found online at https://doi.org/10.1016/j.jmrt.2022.06.171.

REFERENCES

[1] Knipling KE, Dunand DC, Seidman DN. Criteria for developing castable, creep-resistant aluminum-based alloys - a review. Z Metallkd 2006;97:246–65.
[2] Luca ADe, Seidman DN, Dunand DC. Effects of Mo and Mn microadditions on strengthening and over-aging resistance of nanoprecipitation-strengthened Al-Zr-Sc-Er-Si alloys. Acta Mater 2019;165:1–14.
[3] Choi HJ, Bae DH. Creep properties of aluminum-based composite containing multi-walled carbon nanotubes. Scripta Mater 2011;65:194–7.
[4] Balanetskyy S, Pavlyuchkov D, Velikanova T, Grushko B. The Al-rich region of the Al–Fe–Mn alloy system. J Alloys Compd 2015;619:211–20.
[5] Graf A. Aluminum alloys for lightweight automotive structures. In: Mallick PK, editor. Materials, design and manufacturing for lightweight vehicles. 2nd. ed. Elsevier; 2021. p. 97–123.
[6] Que Z, Zhou Y, Wang Y, Mendis CL, Fan Z. Effects of Mg addition on the Al6 (Fe, Mn) intermetallic compounds and the grain refinement of α-Al in Al-Fe-Mn alloys. Mater Charact 2021;171:110758.
[7] Azarniya A, Taheri AK, Taheri KK. Recent advances in ageing of 7 xxx series aluminum alloys: a physical metallurgy perspective. J Alloys Compd 2019;781:945–83.
[8] Yuan W, Liang Z. Effect of Zr addition on properties of Al–Mg–Si aluminum alloy used for all aluminum alloy conductor. Mater Des 2011;32:4195–200.
[9] Alducci EB, Ceschini L, Messieri S, Wenner S, Holmestad R. Thermal stability of the lightweight 2099 Al-Cu-Li alloy: tensile tests and microstructural investigations after overaging. Mater Des 2017;119:54–64.
[10] Li YJ, Muggerud A, Olsen A, Furu T. Precipitation of partially coherent α-Al(Mn,Fe)Si dispersoids and their strengthening effect in AA 3003 alloy. Acta Mater 2012;60:1004–14.
[11] Muggerud AMF, Mørtsell EA, Li Y, Holmestad R. Dispersoid strengthening in AA3xxx alloys with varying Mn and Si content during annealing at low temperatures. Mater Sci Eng, A. 2013;567:21–8.
[12] Liu K, Chen XG. Development of Al–Mn–Mg 3004 alloy for applications at elevated temperature via dispersoid strengthening. Mater Des 2015;84:340–50.
[13] Li Z, Zhang Z, Chen XG. Microstructure, elevated-temperature mechanical properties and creep resistance of dispersoid-strengthened Al-Mn-Mg 3 xxx alloys with varying Mg and Si contents. Mater Sci Eng, A 2017;708:383–94.
[14] Li YJ, Arnberg L. Quantitative study on the precipitation behavior of dispersoids in DC-cast AA3003 alloy during heating and homogenization. Acta Mater 2003;51:3415–28.
[15] Qian F, Jin S, Sha G, Li Y. Enhanced dispersoid precipitation and dispersion strengthening in an Al alloy by microalloying with Cd. Acta Mater 2018;157:114–25.
[16] Liu K, Ma H, Chen XG. Enhanced elevated-temperature properties via Mo addition in Al-Mn-Mg 3004 alloy. J Alloys Compd 2017;694:354–65.
[17] Liu K, Ma H, Chen XG. Improving the elevated-temperature properties by two-step heat treatments in Al-Mn-Mg 3004 alloys. Metall Mater Trans B 2018;49:1588–96.
[18] Liu K, Chen XG. Influence of heat treatment and its sequence on elevated-temperature properties of Al-Mn-Mg 3004 alloy. Mater Sci Eng, A 2017;697:141–8.
[19] Liu K, Chen XG. Evolution of microstructure and elevated-temperature properties with Mn addition in Al–Mn–Mg alloys. J Mater Res 2017;32:2585–93.

[20] Farkoosh AR, Chen XG, Pekguleryuz M. Interaction between molybdenum and manganese to form effective dispersoids in an Al–Si–Cu–Mg alloy and their influence on creep resistance. Mater Sci Eng, A 2015;627:127–38.
[21] Elgallad EM, Liu K, Zhang Z, Chen XG. Effect of transition elements on dispersoid formation and elevated-temperature mechanical properties in 6082 aluminum alloy. Philos Mag A 2021;101:96–116.
[22] Chaijaruwanich A, Dashwood R, Lee P, Nagaumi H. Pore evolution in a direct chill cast Al–6 wt.% Mg alloy during hot rolling. Acta Mater 2006;54:5185–94.
[23] Gajakosh Ak, Keshavamurthy R, Jagadeesha T, Kumar RS. Investigations on mechanical behavior of hot rolled Al7075/TiO2/Gr hybrid composites. Ceram Int 2021;47:14775–89.
[24] Wang B, Zhang J, Xiao C, Song W, Wang S. Analysis of the evolution behavior of voids during the hot rolling process of medium plates. J Mater Process Technol 2015;221:121–7.
[25] Ma K, Liu Z, Zhang X, Xiao B, Ma Z. Fabrication of high strength carbon nanotube/7055Al composite by powder metallurgy combined with subsequent hot extrusion. Sci China Technol Sci 2021;64:1081–91.
[26] Zhang Y, Jin W, Hao X, Qiu F, Zhao Q. Improving elevated-temperature strength of an Al–Mn–Si alloy by strain-induced precipitation. Metals 2018;8:446.
[27] Wang XG, Li QS, Wu RR, Zhang XY, Ma LY. A review on superplastic formation behavior of Al alloys. Adv Mater Sci Eng 2018;2018:1–17.
[28] Zindal A, Jain J, Prasad R, Singh SS. Effect of pre-strain and grain size on the evolution of precipitate free zones (PFZs) in a Mg-8Al-0.5Zn alloy. Mater Lett 2017;201:207–10.
[29] Zhen L, Zhan Z, Chen XG. Effect of metastable Mg_2Si and dislocations on α-Al(MnFe)Si dispersoid formation in Al-Mn-Mg 3 xxx alloys. Metall Mater Trans A 2018;49:5799–814.
[30] Cabibbo M, Evangelista E, Vedani M. Influence of severe plastic deformations on secondary phase precipitation in a 6082 Al-Mg-Si alloy. Metall Mater Trans A 2005;36:1353–64.
[31] Huang W, Liu Z, Xia L, Xia P, Zeng S. Severe plastic deformation-induced dissolution of θ" particles in Al–Cu binary alloy and subsequent nature aging behavior. Mater Sci Eng, A 2012;556:801–6.
[32] Nam C, Han J, Chung Y, Shin M. Effect of precipitates on microstructural evolution of 7050 Al alloy sheet during equal channel angular rolling. Mater Sci Eng, A 2003;347:253–7.
[33] Kim HW, Kang SB, Tsuji N, Minamino Y. Elongation increase in ultra-fine grained Al–Fe–Si alloy sheets. Acta Mater 2005;53:1737–49.
[34] Hu N, Xu XC, Zhang ZZ, Qu X. Effect of re-dissolution of severely deformed precipitated phase on mechanical properties of Al-Cu alloy. Chin J Nonferrous Metals 2010;20:1922–31.
[35] Kaufman JG. Properties of aluminum alloys: tensile, creep, and fatigue data at high and low temperatures. Materials park: ASM International; 1999.